nature communications

Article

https://doi.org/10.1038/s41467-025-57857-9

Galvanic leaching recycling of spent lithium-ion batteries via low entropy-increasing strategy

Received: 18 August 2024

Accepted: 5 March 2025

Published online: 11 March 2025

Check for updates

Jiadong Yu, Yanjun Liu & Jinhui Li

The recycling of spent lithium-ion batteries can effectively mitigate the environmental and resource challenges arising from the escalating generation of battery waste and the soaring demand for battery metals. The existing mixing-then-separating recycling process is confronted with high entropy-increasing procedures, including crushing and leaching, which result in irreversible entropy production due to the decrease in material orderliness or heavy chemical consumption, thereby hindering its thermodynamic efficiency and economic viability of the entire recycling process. Herein, we propose a galvanic leaching strategy that leverages the self-assembly of $LiNi_{0.6}Co_{0.2}Mn_{0.2}O_2$ particles with their inherent aluminium foil current collectors in spent lithium-ion batteries, creating a primary cell system capable of recovering battery metals without pre-crushing or additional reductants. Under the theoretical potential difference of up to 3.84 V, the electrons flow and charge aggregation effectively achieve the valence state reduction, crystal phase transition and coordination environment change of the hard-to-dissolve metal components, contributing to over 90% battery metals recovery and a nearly 30-fold increase in leaching kinetics. Environmental-economic assessments further indicate that this strategy reduces energy consumption and carbon emissions by 11.36%-21.10% and 5.08%-23.18%, respectively, compared to conventional metallurgical methods, while enhancing economic benefits by 21.14%-49.18%.

Lithium-ion batteries (LIBs) play a pivotal role in the global transition to cleaner energy, contributing significantly to achieving a more sustainable planet[1,2]. Nevertheless, the extensive production of LIBs has consumed 70% of global cobalt (Co) resources[3], while the rapid growth of battery waste necessitates urgent disposal strategies[4]. Consequently, the recycling of spent LIBs is essential for ensuring the continued availability of critical raw materials and supporting the sustainable development of the new energy sector[5]. Despite recent advancements in traditional metallurgical recycling processes, the lack of systematic cognitive improvement has made it difficult to further improve their thermodynamic efficiency and economic-environmental benefits[6]. A fundamental principle of thermodynamics dictates that in isolated systems, spontaneous reactions are invariably associated with an irreversible increase in entropy. In terms of LIBs recycling, the high entropy-increasing process will reduce the energy efficiency, promote the release of waste heat and the generation of additional waste, and lead to material mixing, thereby compromising the purity of the recycled products[7]. Therefore, understanding the process entropy changes is vital for optimizing battery recycling processes in a systematic manner. By designing more efficient recycling processes that minimize entropy production, there is an opportunity to enhance resource recovery

State Key Joint Laboratory of Environment Simulation and Pollution Control, School of Environment, Tsinghua University, Beijing, China.
e-mail: jinhui@tsinghua.edu.cn

while reducing energy consumption and mitigating the economic-environmental burden of the recycling industry.

The positive electrodes of LIBs, abundant in lithium (Li) and Co, are securely bonded to an aluminum (Al) foil carrier using a polyvinylidene fluoride (PVDF) binder to form the positive electrode strip. Conventional recycling methods typically involve crushing and screening to obtain battery powder[8], followed by the removal of Al impurities through alkali leaching[9], gravity separation[10] or color separation[11], and ultimately, acid leaching[12] to recover the battery metals. Among them, the crushing step disrupts the original structural order of LIBs by mechanical means, thus increasing the system entropy. Meanwhile, the leaching process consumes a large amount of chemicals and water, leading to irreversible energy loss and further contributing to environmental entropy. If the positive electrode strips can be introduced into the acid leaching while preserving their original structure, without prior crushing or additional chemical consumption, the entropy production associated with the recycling process can be substantially reduced. In fact, Al foil has been employed as a zero-valent metal reductant to facilitate efficient reductive leaching of positive electrodes[13–15]. Chernyaev et al.[16] and Peng et al.[17] reported that Al foil fragments in spent LIB itself could increase the leaching rate of Li and Co from ~80% to ~100%, but due to the side reactions involving hydrogen evolution, their actual consumption is too high. Joulié et al. found that the ternary positive electrodes could be completely dissolved using Al foil fragments as a reducing agent, whereas this required 24 h[18]. Therefore, while the low entropy-increasing recycling stategy of directly leaching the positive electrode strips appears theoretically feasible, further research is necessary to investigate the impact of hydrogen evolution side reactions on electron reduction efficiency and leaching kinetics within this new system.

Based on the principle of minimum entropy production, this work aims to systematically optimize the hydrometallurgical recycling process for spent LIBs, thereby enabling the efficient and rapid recovery of battery metals. Herein, we demonstrate that the waste $LiNi_{0.6}Co_{0.2}Mn_{0.2}O_2$ (NCM) electrodes can form a primary cell system with the Al foil current collectors inherent in spent LIBs to induce a targeted transfer of electrons only for the reductive deconstruction of layered NCM electrodes, instead of generating hazardous H_2 or releasing organofluorine contamination. We refer to this low entropy-increasing recycling strategy as the galvanic leaching method, which is shown to enhance the recovery rates of Li to over 99% and transition metals to over 90%. More importantly, the electron reduction efficiency is increased by ~25 times, and the leaching kinetics are improved by ~30 times. Environmental-economic assessments further reveal that the galvanic leaching method offers unique advantages in terms of energy saving, carbon reduction and economic benefits, highlighting its potential as a more sustainable and efficient alternative for LIB recycling.

Results

Thermodynamic feasibility analysis and kinetic evidence

We model the NCM electrode materials as a mixture of Ni_2O_3, Co_2O_3 and MnO_2[18], and determine the optimal reductant by comparing their Gibbs free energy changes for reacting with different reductants, including H_2O_2, $NaHSO_3$, and Al foil. The possible reaction equations and their expressions for Gibbs free energy change ($\Delta_r G_T^\theta$) as a function of temperature (T), are shown in Fig. S1 and Supplementary Note 1. Given that these reactions predominantly occur in aqueous solutions, the reaction temperature range is considered to be 273–373 K[19,20]. The results indicate that the Gibbs free energy curves for redox reactions using Al foil as a reductant are lower than those of both H_2O_2 and $NaHSO_3$. It is theoretically proved that the leaching effect of the Al-metal reductant inherent in spent LIBs is better than that of the common external reductants. Furthermore, the Gibbs free energy of each redox reaction of transition metal oxides using Al foil as a reducing agent is lower than that for the hydrogen evolution reactions between Al foil and acid, as shown in Fig. 1a. This suggests that, as long as Al foil is kept in contact with NCM particles, electrons released from Al foil are preferentially transferred to NCM particles, ensuring that the reduction of NCM is completed before any significant hydrogen gas (H_2) generation occurs in the acid solution.

The galvanic leaching system in this work involves a series of redox reactions, where the transition metal oxides act as the negative electrode, and the Al foil serves as the positive electrode. In this system, the electrons gained and lost during the reactions are directly transferred through the solid-solid contact surface without adding either a salt bridge or a power supply. We have also calculated the potential (E) of the redox pairs formed by Ni, Co, Mn, Al and their respective oxides, as shown in Table 1, and the corresponding expression is given below:

$$E = \varphi_+ - \varphi_- \tag{1}$$

The specific potential (E) for the reactions of Al with transition metal oxides are as follows:

$$Ni_2O_3 + \frac{2}{3}Al + 6H^+ \rightarrow 2Ni^{2+} + \frac{2}{3}Al^{3+} + 3H_2O \tag{2}$$

$$E = \varphi_{(Ni_2O_3/Ni^{2+})} - \varphi_{(Al^{3+}/Al)} = 3.84V \tag{3}$$

$$Co_2O_3 + \frac{2}{3}Al + 6H^+ \rightarrow 2Co^{2+} + \frac{2}{3}Al^{3+} + 3H_2O \tag{4}$$

$$E = \varphi_{(Co_2O_3/Co^{2+})} - \varphi_{(Al^{3+}/Al)} = 3.39V \tag{5}$$

$$MnO_2 + \frac{2}{3}Al + 4H^+ \rightarrow Mn^{2+} + \frac{2}{3}Al^{3+} + 3H_2O \tag{6}$$

$$E = \varphi_{(MnO_2/Mn^{2+})} - \varphi_{(Al^{3+}/Al)} = 2.94V \tag{7}$$

The potential E of the above three reactions is much higher than the formation boundary value of 0.5 V for the primary cell reaction[21,22]. From an electrochemical perspective, this substantial potential difference of 2.94–3.84 V forces electrons to preferentially flow through the solid-solid interface, thereby promoting the reduction of NCM electrodes while preventing the generation of hydrogen gas, as shown in Fig. 1b. It is worth noting that the Li^+ ions embedded in the NCM electrode will move in the opposite direction to the electron flow, and be attracted by the charge accumulating near the Al foil and tend to gather in close proximity to it. We have also submitted a Supplementary Movie 1 showing the current and voltage measurement obtained using an ammeter in the actual experiments, further demonstrating the viability of the NCM electrodes with the inherent Al foil current collectors in forming a functional primary cell.

It is necessary to note that in the galvanic leaching system, the leaching rates of Li, Ni, Co and Mn elements are 3–4 times higher when using hydrochloric acid (HCl) compared to sulfuric acid (H_2SO_4), as shown in Fig. 1c. This is because SO_4^{2-} and Al^{3+} ions readily form $Al_2(SO_4)_3$ precipitation, which can adhere to the surface of Al foils and hinder the contact reaction between H^+ ions and Al foils, as illustrated in Fig. S2. Detailed condition optimization experiments (Fig. 1d–f) show that under 2 mol/L HCl, 200:1 mL/g and 60 °C, the HCl-induced galvanic system can achieve a Li leaching rate of ~99%, and leaching rates for Ni, Co and Mn of 91.62%, 95.15%, and 94.19%, respectively. More importantly, it is observed that only ~2.90% of the electrons in

https://doi.org/10.1038/s41467-025-57857-9

the high entropy-increasing system (the crushed positive electrode strips from spent LIBs[16–18]) are engaged in the redox reaction of the NCM electrode. This is much lower than the 79.97% electron participation in the galvanic system, representing a 25-fold improvement in electron efficiency, as shown in Fig. 2g. The further leaching kinetics in Figs. S3–4, Tables S1–5 and Supplementary Note 2 show that the activation energies for Ni, Co and Mn drastically decrease from 56.35, 73.95l and 58.51 kJ/mol in the high entropy-increasing system to 31.9,

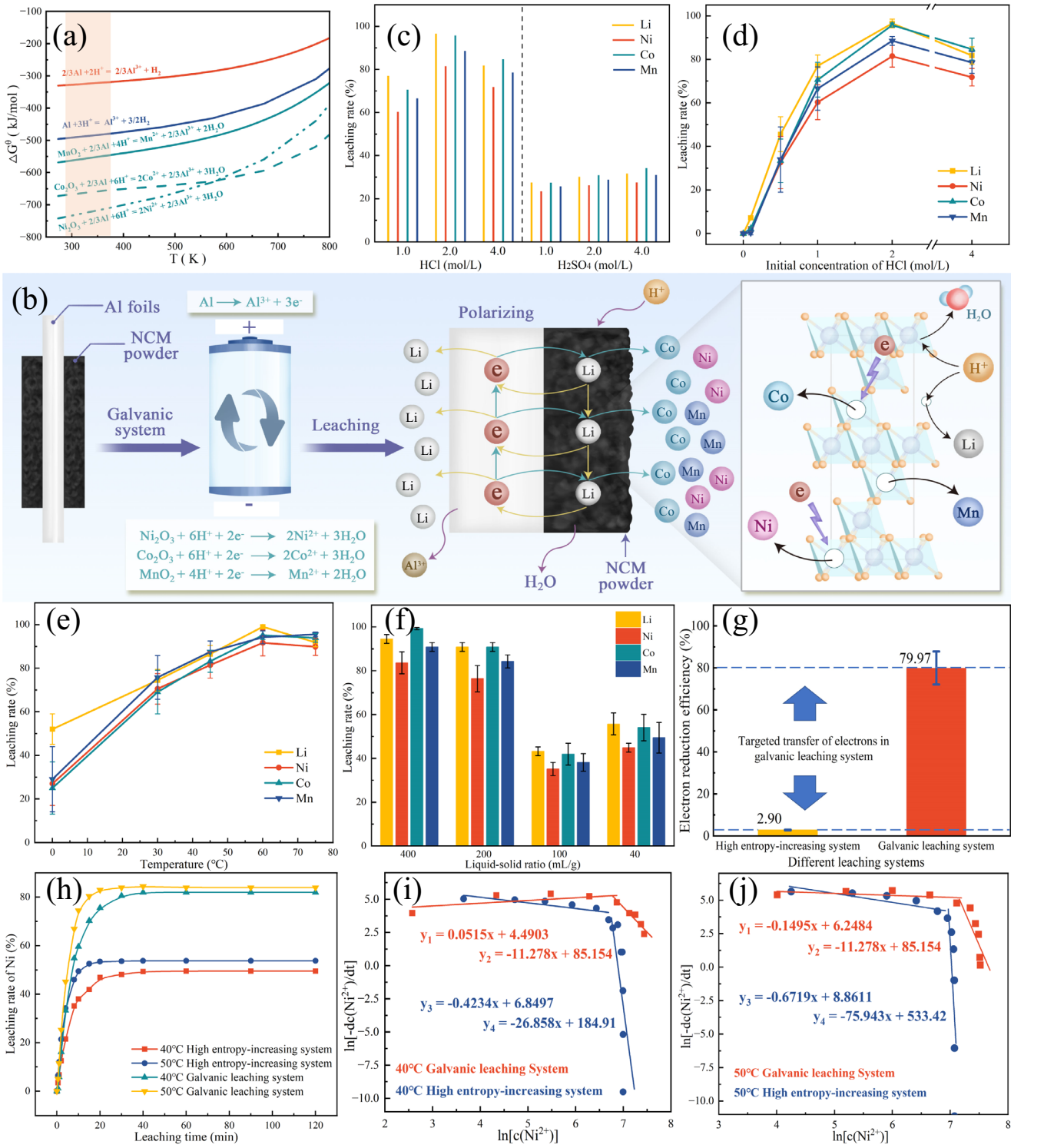

Fig. 1 | Improved metal recovery in galvanic leaching systems. a The thermodynamic analysis based on Gibbs free energy. **b** The design principle of self-assembly galvanic leaching system from spent lithium-ion batteries. **c** The actual recovery effect of galvanic leaching systems excited by different concentrations of HCl and H_2SO_4. Condition optimization of galvanic leaching system from **d** initial concentration of HCl, **e** liquid–solid ratio and **f** leaching temperature. The error bars reflect the standard deviations from at least three individual measurements. The same below. **g** Electron reduction efficiency under the optimal leaching parameters: 2 mol/L HCl, 200:1 mL/g and 60 °C. **h** The kinetic leaching rate of Ni. Relationship between kinetic nickel leaching rate and the concentration of Ni^{2+} in the leachate at **i** 40 °C and **j** 50 °C. The error bars in **d**–**g** reflect the standard deviations from at least three individual experiments, and the data are expressed as mean ± s.e.m.

Table 1 | Redox potentials of the related elements

Redox pairs	Reaction equation	φ vs. SHE	
(Ni_2O_3/Ni^{2+})	$Ni_2O_3 + 2e^- + 6H^+ \rightarrow 2Ni^{2+} + 3H_2O$	+2.13 V	(8)
(Co_2O_3/Co^{2+})	$Co_2O_3 + 2e^- + 6H^+ \rightarrow 2Co^{2+} + 3H_2O$	+1.68 V	(9)
(MnO_2/Mn^{2+})	$MnO_2 + 2e^- + 4H^+ \rightarrow Mn^{2+} + 2H_2O$	+1.23 V	(10)
(Al^{3+}/Al)	$Al^{3+} + 3e^- \rightarrow Al$	-1.71 V	(11)

39.31 and 37.94 kJ/mol in the galvanic system. In contrast, the activation energy for Li increases from 16.94 to 44.70 kJ/mol, due to the charge binding of Li^+ ions within the primary cell system. Compared to the high entropy-increasing system, the galvanic system achieves over a 30-fold increase in the dissolution rate of battery metals, such as nickel, at 40–50 °C. Additionally, the high dissolution rate is maintained for a longer period until the end of the reaction, as shown in Figs. 1h–j, S5 and S6 and Supplementary Note 3. Overall, the galvanic leaching system can simultaneously improve the metal dissolution rate and recovery efficiency by increasing the electron reduction efficiency and lowering the reaction activation energy. This improvement is crucial for making the recycling process more efficient and sustainable, contributing to the broader goal of reducing energy consumption and environmental impact in the recycling of spent LIBs.

Morphological and lattice evolution in reductive deconstruction process

The waste NCM electrode particles consist of secondary aggregates of transition metal oxides, exhibiting continuous and smooth surfaces, as shown in Fig. 2a. In the galvanic leaching system, the surface of the waste positive electrode particles firstly undergoes dissolution and cracking (Fig. 2b), and then the dissolution progresses inward, forming cavities within the particles (Fig. 2c). As the galvanic leaching process continues, the cavities inside the particles expand and deepen, as shown in Fig. 2c–e. Eventually, only an organic structural framework, composed of C/F/O-containing components, remains in Figs. 2f and S7. The reason for the emergence of such cavities from the center of particles will be discussed in detail in subsequent sections.

A field emission electron probe micro-analyzer (FE-EPMA) has been employed to characterize the morphological evolution of the entire positive electrode strip from the surface to the bulk, over the course of leaching. The observed morphology in Figure S8 and Supplementary Note 4 reveal that the width of the positive electrode strip initially swells from ~145 μm to ~250 μm, and then shrinks to ~110 μm as leaching progresses. We select Co and F as the representative elements of NCM particles and PVDF binder, respectively. Figure S9 shows that the NCM particles are tightly adhered to the Al foils via the PVDF binder, which corresponds to the positive electrode (middle Al foils) and the negative electrode (NCM particles on both sides) of a primary cell system. The average intensity of Co in the positive electrode strip is 76, while the intensity of F is only 0.53, indicating that a small amount of PVDF-containing organic framework does not completely shield the reaction between NCM particles and HCl. After 5-min leaching, the overall Co content decreases rapidly, as shown in Fig. 2h, and the residual content of Co in the middle is significantly higher than that on the surface. After 10-min leaching, the Co content continues to decrease, as shown in Fig. 2k, and the remaining high Co-containing particles are predominantly enriched on both sides of the middle Al foils. The shell remnants observed on the outer surface of the positive electrode strips in Fig. 2g, j are consistent with the cavity structure described earlier, further confirming that although the Al foil is in contact with the NCM particles internally, the electron transfer through the galvanic reaction leads to the reductive deconstruction of the outer NCM particles. After 40-min leaching, Co elements were almost undetectable, as shown in Fig. 2m-n, proving that the galvanic leaching system can effectively dissolve NCM particles within 40 min.

It is exciting to note that the F-containing PVDF binder can be consistently detected with constant intensity throughout the leaching process, as shown in Fig. 2i, l, o. This indicates that the galvanic leaching system only dissolves the metal materials while leaving the organic structure largely intact. As a result, this system effectively suppresses fluoride contamination in the leaching solution. The remaining binder, with conductive carbon black cured within it, retains its good electrical conductivity, which plays a crucial role in achieving a high electron reduction efficiency (80%) in the galvanic leaching system.

High resolution transmission electron microscope (HRTEM) has been employed to characterize the microscopic transformation of the lattice composition of a single NCM particle from the surface to the bulk at the nanoscale. The high-angle annular dark field-scanning transmission electron microscopy (HAADF-STEM) images in Fig. 3a, d, g reveal that the electron reflection from high-energy metal inside the raw materials of spent NCM particles is homogeneous. However, after 5-10 min galvanic leaching, a clear shell-kernel delamination phenomenon becomes apparent. The electron diffraction patterns in Fig. 3b, e, h show that, as leaching progresses, the lattice configuration of the spent NCM particles gradually transforms from a lamellar structure characteristic of the original R-3m hexagonal crystal system to a spinel phase, a mixture of R-3m and Fm-3m, and ultimately evolves into a pure rock-salt structure with an Fm-3m face-centered cubic crystal system[23,24]. The detailed HRTEM images and their corresponding fast Fourier transform (FFT) patterns of the marked areas in Fig. 3c, f, i and Figures S10–15 suggest that galvanic leaching induces a gradual transformation of the lamellar $LiNiO_2$ lattice of individual NCM particles from the surface to the bulk into a rock-salt NiO lattice. Their interplanar spacing of the lattice decreases from the typical value of 0.48 nm, to about 0.23 nm[25,26]. Based on this observed lattice transformation, it can be inferred that the substantial potential difference of 2.94–3.84 V (as shown in Fig. 3j) induces the Li^+ ions in the layered octahedral unit cell to undergo ionic hopping, resulting in the forming of lithium vacancies[27]. Concurrently, transition metal (TM) ions with a similar ionic radius occupy these vacancies through the same hopping pathway, leading to the formation of a spinel/rock-salt structure. This enhanced cation mixing accelerates the sequential leaching of both Li^+ and TM ions from the crystal lattice into the liquid phase. Furthermore, significant etching pores and grooves emerge between adjacent crystal planes of the NCM particles during the 5–10 min leaching period. The degree of corrosion within the interior of the particles is greater than that on the outer surfaces. This phenomenon is attributed to the current accumulation or charge aggregation inside the particles, caused by the mismatch between the electron transport rate and the crystal reduction rate. This internal charge buildup leads to surface lattice transformation and internal lattice collapse, which is similar to the phenomenon of material expansion, heat generation, and lattice damage caused by reversing the connection of the positive and negative electrodes in a battery[28–30].

Mechanism of the improved metal recovery in galvanic leaching system

According to the element analysis and X-ray diffractometer (XRD) analysis (Fig. 4a, b), the raw materials are waste $LiNi_{0.6}Co_{0.2}Mn_{0.2}O_2$ electrodes with a $LiNiO_2$ crystal phase and transformed into a NiO phase with organic residues including carbon black conductor after galvanic leaching[31], which is consistent with previous HRTEM analyses. Figure 4c shows that the gradual disappearance of the main (003) peak of the NCM electrodes as leaching time increases, demonstrating the effective deconstruction of the crystal structure by the galvanic leaching system. Local magnified XRD patterns in Fig. 4d show that the (104), (018), and (110) peaks of NCM electrodes decrease and shift towards smaller values of 2θ, indicating stretching and progressive breakdown of the crystal planes in the non-perpendicular directions.

https://doi.org/10.1038/s41467-025-57857-9

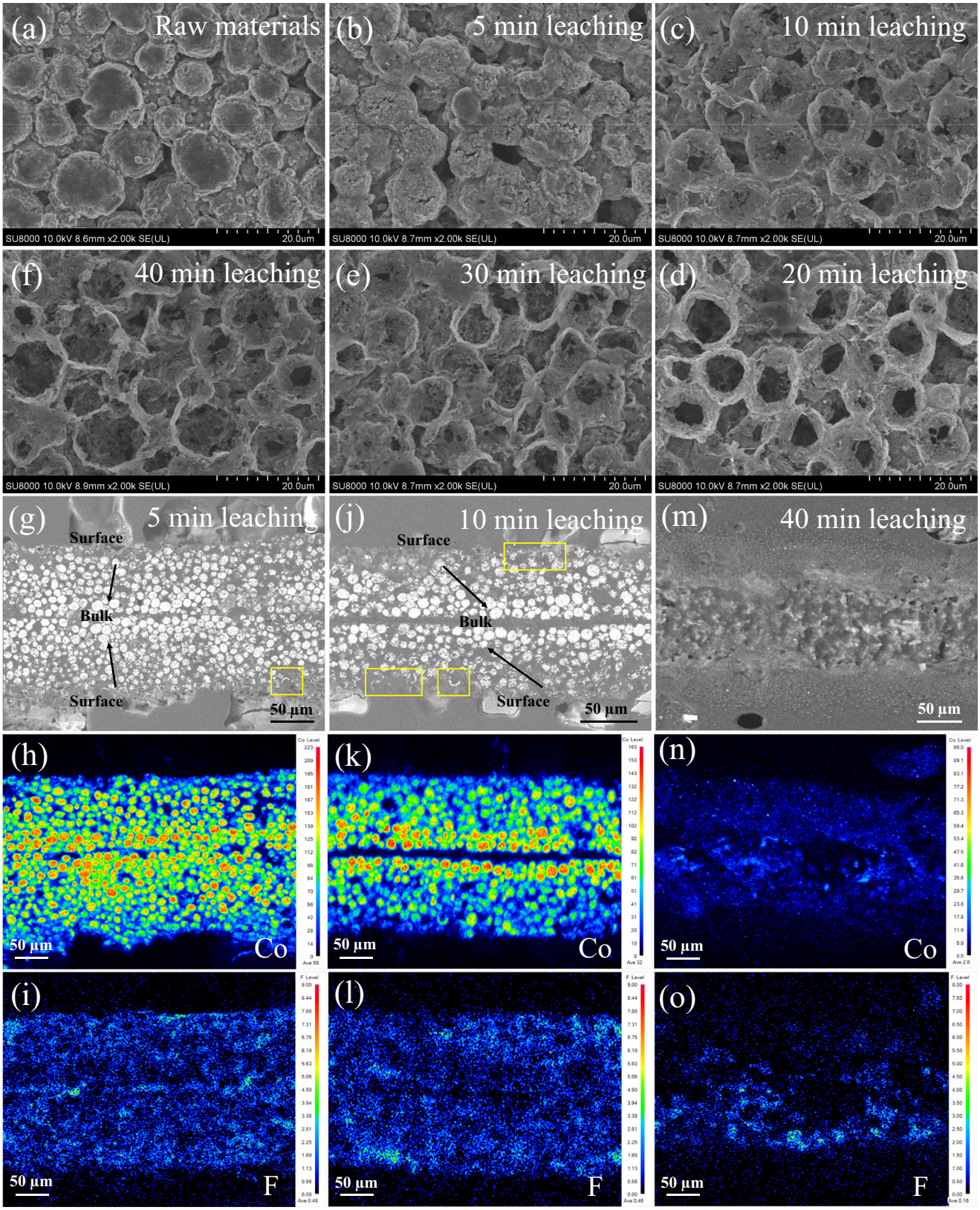

Fig. 2 | Migration evolution of surface morphology and elemental distribution during galvanic leaching process. SEM image of NCM particles with galvanic leaching times of **a** 0 min, **b** 5 min, **c** 10 min, **d** 20 min, **e** 30 min and **f** 40 min. **g-i** are the micro-morphology of particles from the surface to the bulk of NCM electrode strips at a galvanic-leaching time of 5 min, along with the corresponding elemental distribution of cobalt and fluorine, while **j**–**l** and **m**–**o** represent the situations at leaching times of 10 min and 40 min, respectively. **g**–**i, j**–**l**, and **m**–**o** are samples from three parallel experiments, all conducted under the leaching condition of 2 mol/L HCl, 200:1 mL/g and 60 °C. **g**–**o** The leached positive electrode strip is placed in a mold with an upright straightener, and then cured with poured epoxy resin to form a hard resin block, and finally is sandblasted and polished to reveal its cross-section.

https://doi.org/10.1038/s41467-025-57857-9

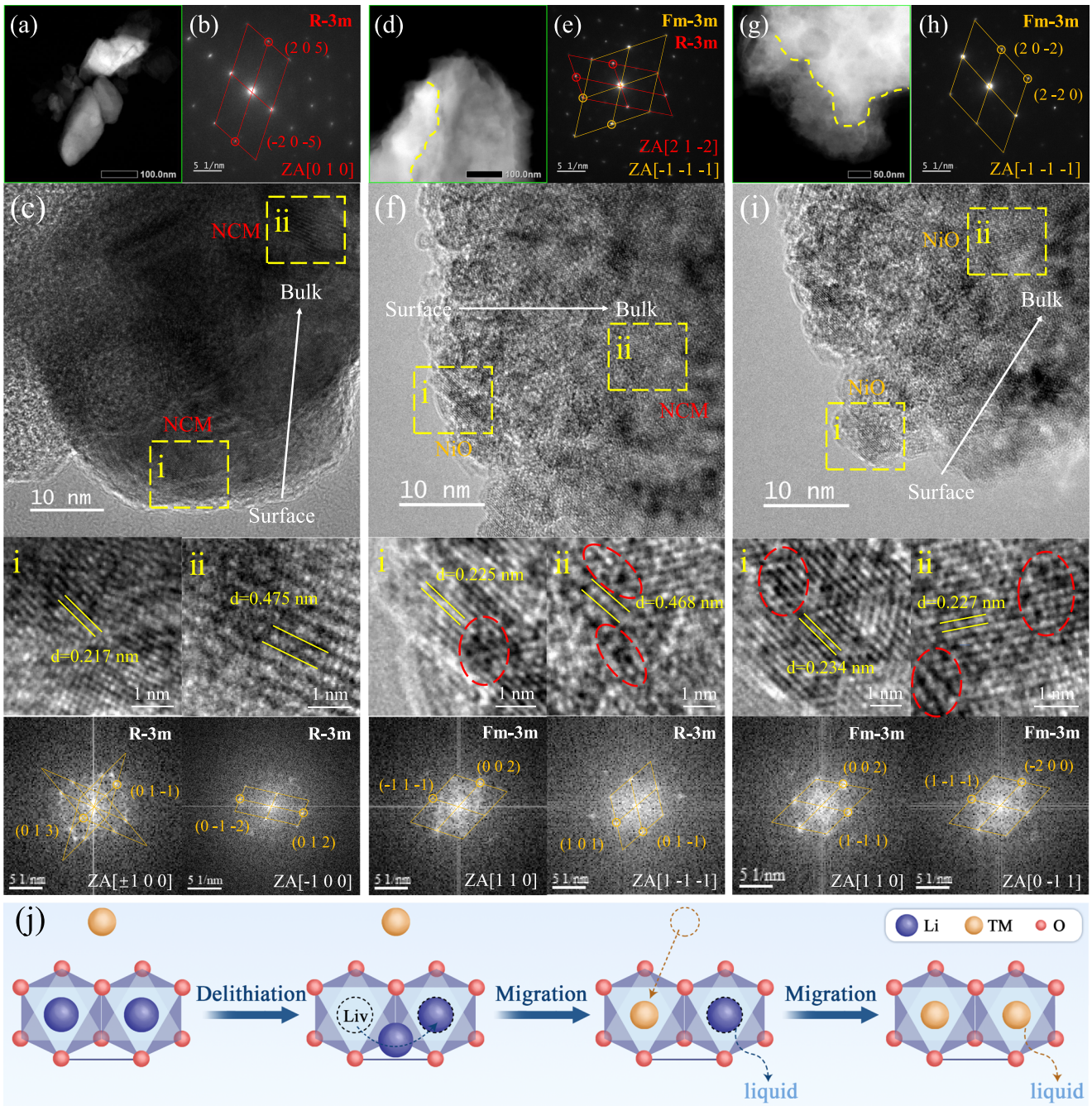

Fig. 3 | Microstructural transformation of spent NCM electrode particles in galvanic leaching system. a–c Raw materials of spent NCM particles. **d–f** 5-min leaching products. **g–i** 10-min leaching products. **a**, **d**, **g** are HAADF-STEM images. **b**, **e**, **h** are electron diffraction patterns taken directly from TEM equipment. **c**, **f**, **i** are HRTEM image of different leaching products and the corresponding FFT patterns analyzed by Digital Micrograph. **j** The degradation mechanism of NCM electrodes during galvanic leaching.

This crystal decomposition is a key physical means to improve the leaching of metals from spent LIBs, while the chemical driving force behind this transformation is valence migration. X-ray photoelectron spectroscopy (XPS) analysis of Ni 2p, conducted after 0–1200 s etching in Fig. 4e, f, shows that the NCM particles after 5 min galvanic leaching exhibit a trend of valence state transition from +3 to +2 from the surface to the bulk[32], with the atomic content of Ni in the bulk being higher than that at the surface. The reason is that the reduced Ni^{2+} on the particle surface preferentially dissolves into the HCl solution, leaving behind insoluble Ni^{3+} in the surface layer. To avoid the influence of surface metal dissolution, XPS analysis has been performed 240 nm beneath the particle surface before and after galvanic leaching, as shown in Fig. 4g-h, with each 300-s etching step corresponding to a depth of 60 nm. It shows that a 10 min galvanic leaching is sufficient to reduce the 100% Ni^{3+} environment inside the NCM particles to a mixture of 25.08% Ni^{2+} and 74.92% Ni^{3+}, and the Ni content of the 10 min leaching particles is decreased by 48.15%, from 5.4% to 2.8%. These evidences indicate that the 10 min galvanic leaching can dissolve 48.15% of nickel in the surface layer of NCM particles within 240 nm, and reduce 25.08% of the high-valence nickel in the remaining particles to a lower valence state.

The above XPS spectra provide insight into the valence state transitions occurring at the the surface layer of spent NCM electrodes, and in the following, we further investigate the transformation of the

https://doi.org/10.1038/s41467-025-57857-9

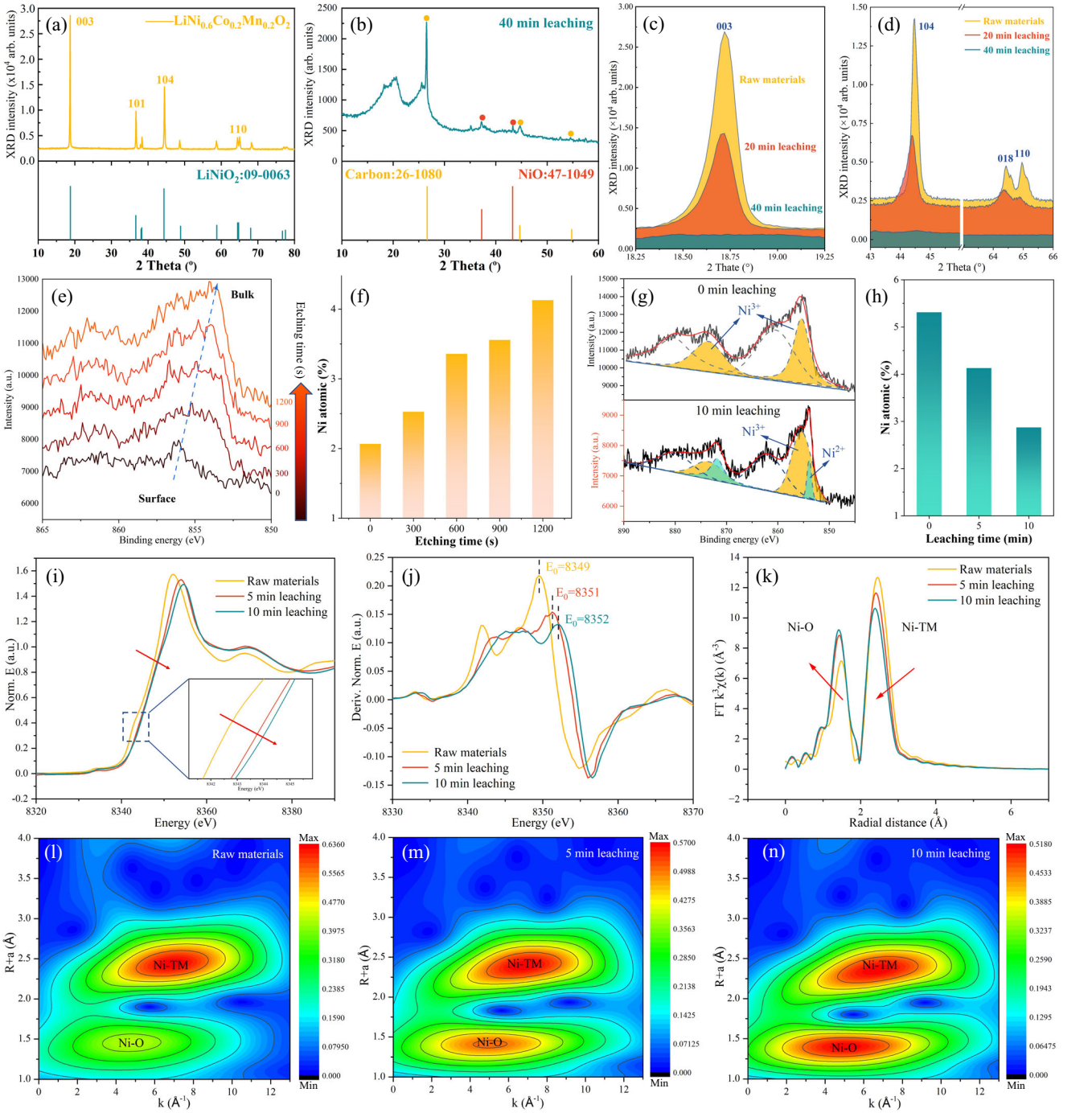

Fig. 4 | Mechanism of improved metal recovery in galvanic leaching system. XRD pattern of **a** raw materials and **b** 40 min leaching products. The local magnification of **c** 003 peak and **d** $2\theta = 43–66°$ at different leaching times. **e** Ni 2*p* XPS spectra of 5 min leaching products by in-depth etching and **f** the corresponding Ni atomic percent from the surface to the bulk. **g** Ni 2*p* XPS spectra inside raw materials and 10 min leaching products, measured after 1200 s surface etching, respectively. **h** The atomic percent of Ni inside different leaching products, measured after 1200 s surface etching. **i** Ni K-edge XANES. **j** The first derivative of XANES. **k** Ni K-edge extended X-ray absorption fine structure spectra. **l**–**n** The 2D contour Fourier-transformed Ni K-edge EXAFS analysis. All leaching products were obtained from galvanic leaching system with the optimal leaching parameters.

internal chemical state of the leaching particles. As illustrated in the Ni K-edge X-ray absorption near edge structure (XANES) spectrum in Fig. 4i, galvanic leaching induces a notable change in the pre-edge of NCM particles, characterized by a rightward shift. This shift suggests an increase in the Ni^{2+} content within the sample[33,34]. With the increase of leaching time, the E_0 value in the first derivative of the energy edge increases from 8349 eV to 8352 eV (Fig. 4j), which proves the rising oxidation state of Ni in the bulk structure of the galvanic leaching products[35]. The k^3-weighted Fourier transforms of extended X-ray absorption fine structure (EXAFS) spectrum in Fig. 4k show that with prolonged leaching, the coordination shell corresponding to the Ni-O scattering path increases, while the coordination shell related to the Ni-transition metal (Ni-TM) scattering path decreases. Combined with the EXAFS fitting parameters in Table S6, it domonstrates that during the galvanic leaching process, the coordination environment of Ni is unstable, and the coordination bonds between Ni and transition

metals diminish, gradually transitioning to Ni–O coordination bonds, which can also be confirmed by the 2D contour Fourier-transformed Ni K-edge EXAFS in Fig. 4l–n. Consequently, under a potential difference of up to 3.8 V in the primary battery system, electrons released from Al foil pass through the organic conductor and enter the NCM particles, as shown in Fig. S16. This electron flow leads to preferential reduction and dissolution of the transition metal oxides within the NCM particles, ultimately resulting in the formation of cavity structures, as shown in Fig. 2a–f. It is the electron flow in the surface layer and the charge aggregation within the bulk of the particles that facilitate the reduction of valence states, crystal phase transitions, and alterations in coordination environments of the spent positive electrode particles, from the surface to the bulk. This mechanism underpins the rapid and efficient dissolution and recovery of metals during the galvanic leaching process.

Environmental impact assessment and techno-economic analysis

Based on the galvanic leaching principle, we have designed a scalable upcycling process of spent NCM batteries into new Al-doped $LiNi_{0.8}Co_{0.1}Mn_{0.1}O_2$ electrodes, and the simple schematic diagram is shown in Fig. 5a. It should be noted that the process feed is positive electrode strips containing Al foil and partially detached positive electrode powder with $LiCoO_2$ or $LiNi_xCo_yMn_zO_2$ ($x+y+z=1$) as the crystalline phase, which may originate from manual disassembly of spent LIBs or from positive electrode scraps during battery production. With the improvement of the automated dismantling equipment as shown in Fig. S17 and the increasing attention from more recycling enterprises, the feed source will steadily increase in the near future. The key step of this scalable upcycling process is to compress the crushed NCM electrodes and Al foils into a cake-like galvanic body, which does not cause a significant process entropy change because it does not induce impurity mixing. The industrial computerized tomography images in Fig. S18 show there is extensive close contact between the Al foil and the NCM electrode inside the galvanic body, forming multiple primary cell systems that are similarly arranged in series and parallel order. Thanks to the action of ~20 MPa pressure and the good ductility of Al foil, this galvanic body can withstand the corrosive effects of higher concentration of HCl. Consequently, the liquid-to-solid ratio in the subsequent leaching process can be reduced from 200 ml/g to 10 ml/g, equivalent to a slurry concentration of 100 g/L, and thus the leaching rates of Li, Ni, Co, Mn and Al can be optimized to over 90%. Furthermore, Figs. S19, 20 and Table S7 demonstrate that the regenerated Al-doped NCM electrodes exhibit a dense crystalline state, favorable elemental distribution, and satisfactory electrochemical cycling performance, thereby substantiating the feasibility of this upcycling process of spent LIBs.

We tried to evaluate the environmental impact and economic feasibility of the galvanic leaching method (Galvanism, Figure S21) for the recycling of spent LIBs through the *EverBatt* 2023 model[36] proposed by Argonne Laboratories in the United States, and compare it with high entropy-increasing strategies including conventional pyrometallurgical (Pyro, Figure S22) and hydrometallurgical (Hydro, Fig. S23) recycling routes, and the obtained data are shown in Tables S8–S13. Conventional pyrometallurgy requires heating the spent LIBs to 800 °C and holding that temperature for 3–5 h to burn off the organic matter and recover metals as alloys. Although this method consumes the least amount of HCl and NaOH, its electrical energy consumption is several times higher than that of hydrometallurgical methods, and thus corresponds to the heavy energy consumption and GHG emissions, which reaches 3650 MJ/kg cell and 29.21 kg/kg cell, respectively, as shown in Fig. 5b, c. Compared with the conventional metallurgical methods, the galvanic leaching system not only inherits the mild reaction conditions of hydrometallurgy, but also requires no external reducing agent, and has the unique advantages of short reaction time and high atomic utilization efficiency, where ~95% Li^+ and ~100% Al^{3+} in spent LIBs will be incorporated into the final regenerated positive electrode materials. Thus it has the lowest energy consumption and GHG emissions, which are 21.10% and 23.18% lower than those of the pyrometallurgical route, and 11.36% and 5.08% lower than those of the hydrometallurgical route. Figure 5d shows the emissions of various gaseous pollutants. It can be found that the emissions of acid gases such as NO_x and SO_2 from pyrometallurgical route are much higher than those of other methods, while the emissions of VOC, CH_4, and CO_2 are comparable among these three routes. Figure 5e, f illustrate the product value, energy costs, chemical costs, waste disposal costs and final economic benefits of the three recycling routes. These data suggest that pyrometallurgical method can cause the volatilization loss of lithium ions, reduce the variety and profit of the recycled products, and also necessitate the addition of more expensive chemicals during the remanufacturing of positive electrode materials, resulting in an economic benefit of only $17.82 /kg cell. Moreover, the galvanic leaching method immobilizes fluorinated pollutants in solid waste, which slightly increases the cost of solid waste disposal. However, it significantly reduces the difficulty and amount of wastewater and exhaust gas treatment, while consuming a lower dose of chemicals. Therefore, its economic benefit is satisfactory, reaching $26.58 /kg cell, which is a 49.18% improvement over the pyrometallurgical route, and a 21.14% improvement over the hydrometallurgical route. With the advancement of membrane treatment technologies[37,38], the recycling of HCl in acid pickling wastewater will become industrializable in the future, which will further enhance the economic and environmental benefits of this galvanic leaching strategy.

Discussion

Entropy production is an inevitable physicochemical process, and the challenge lies in optimizing these processes to minimize the increase in entropy. The process entropy change associated with the LIBs recycling suggests that crushing and leaching are the main stages contribute significantly to the overall entropy increase. Therefore, this work proposes a short-path leaching approach that eliminates the need for pre-crushing and additional reductants, aiming to achieve efficient and rapid recovery of battery metals under a low entropy-increasing environment. Specifically, the waste $LiNi_{0.6}Co_{0.2}Mn_{0.2}O_2$ (NCM) electrodes self-assemble with its bonded Al foil current collector to form a complete primary cell system. This configuration effectively confines free electrons, ensuring that they are involved exclusively in solid-phase redox reactions, rather than escaping into the solution and triggering side reactions such as hydrogen evolution. Thanks to a theoretical potential difference of up to 3.84 V, the electron reduction efficiency increases dramatically from 2.90% to 79.97%. The resulting electron flow and charge aggregation are the main reasons for the crystal deconstruction of the positive electrode materials. This electrochemical action does not compromise the integrity of the organic electrolyte structure between NCM electrode particles, which helps to prevent contamination from solid-phase organic fluorides into the liquid phase system. Under optimal conditions, the recovery rates of Li, Ni, Co and Mn are 99.01%, 91.62%, 95.15%, and 94.19%, respectively. Additionally, the metal dissolution rate is increased more than 30-fold, and this high dissolution rate remains nearly constant throughout the reaction. Through the *EverBatt* 2023 model, this result proves that the energy consumption and carbon emissions of this galvanic leaching strategy are reduced by 11.36%-21.10% and 5.08–23.18%, respectively, compared to conventional metallurgical methods. Moreover, the economic benefit reaches $26.52 /kg cell, representing a 21.37–49.24% improvement. Last but not least, many high-value but difficult-to-recycle urban minerals, such as circuit boards and monitors, face similar high entropy-increasing recycling problem. While shredding is commonly employed due to its simplicity,

https://doi.org/10.1038/s41467-025-57857-9

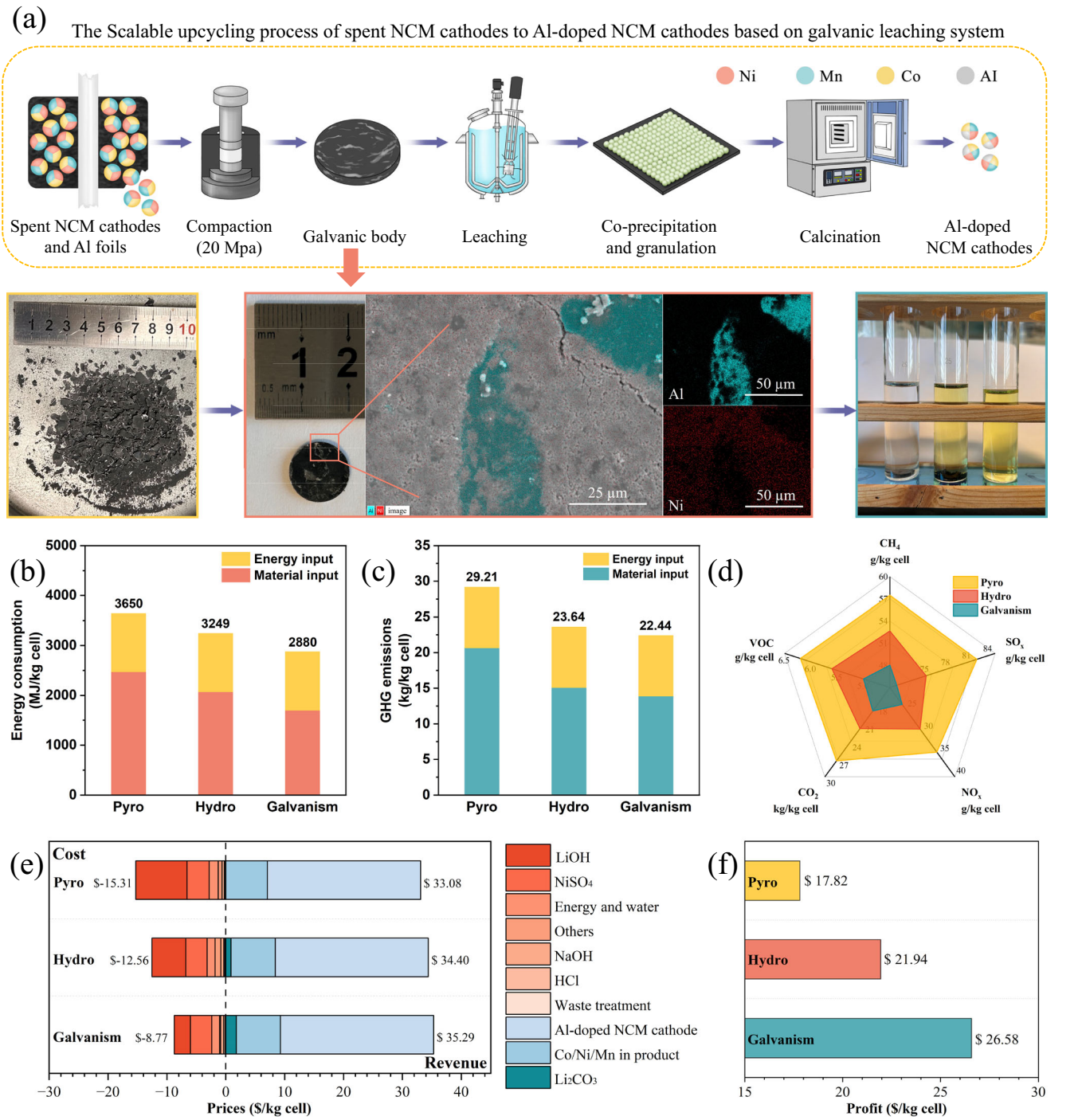

Fig. 5 | Economic and environment analysis. a The simple schematic diagram illustrating the scalable upcycling process from spent NCM batteries to new Al-doped $LiNi_{0.8}Co_{0.1}Mn_{0.1}O_2$ electrode materials, and the specific process flow diagram is shown in Fig. S20. **b** Total energy consumption comparison. **c** Greenhouse gas (GHG) emission comparison. **d** Comprehensive comparison of gaseous pollutants. **e** Cost and revenue of recycling 1 kg of spent LIBs to 1 kg of $LiNi_{0.8}Co_{0.1}Mn_{0.1}O_2$ electrode materials. **f** The final profit of recycling 1 kg of spent LIBs. $ is in US dollars.

it significantly complicates subsequent recycling efforts. This study underscores the importance of process entropy management and its potential to drive technological advancements in urban mining, clean production, and the circular economy.

Methods

Raw materials and pretreatment

The raw materials of spent NCM batteries used in this work came from a pure electric vehicle produced by BYD in 2019, which was donated by GEM Corporation, Ltd. Prior to further processing, the spent NCM batteries were subjected to a short-circuiting procedure to reduce their remaining charge to less than 5%. Subsequently, the batteries were immersed in salt water for 48 h to ensure complete discharge[14], during which lithium ions (Li^+) were driven from the graphite electrodes back to the NCM electrodes[39]. Discharged NCM batteries need to be disassembled in a fume hood, and the intact positive electrode strips should be taken out and ventilated to dry[40,41]. All the chemicals were analytically pure and were purchased by Tsinghua University. The

water used in the experiments was deionized water, which was prepared and quality controlled by the School of Environment, Tsinghua University.

Leaching recovery of spent lithium-ion batteries

In the high entropy-increasing system, the waste NCM electrode strips need to be crushed and dissociated with a shear crusher, and the obtained mixture of NCM electrode powder and Al foil fragments sent to a reactor for acid leaching and dissolution. In a galvanic leaching system, the waste NCM electrode strips are fed directly into the reactor for acid leaching and dissolution, without additional crushing steps. In particular, we explored the theoretical optimum and its mechanism of galvanic leaching by using plastic pins to clamp the positive electrode strip, to prevent separation of the Al foil from the NCM particles. In an expanded application, we granulate the crushed products of spent LIBs, and then leach them with HCl acid; this tight adhesion of the Al foil fragments to the positive electrode particles also produces a leaching effect similar to those of a galvanic leaching system. The preparation method and electrochemical performance testing of the Al-doped $LiNi_{0.8}Co_{0.1}Mn_{0.1}O_2$ electrodes are described in Supplementary Note 5.

Electron reduction efficiency

The electron reduction efficiency is the ratio of the amount of Al dissolved into leaching solution to the total amounts of Ni, Co, and Mn, and can be used to quantitatively analyze the electron targeted transfer involved in redox reactions. With $LiNi_xCo_yMn_zO_2$ (x + y + z = 1) as the active component, $Ni_xCo_yMn_z$ is regarded as the equivalent of Me(III), i.e., $LiMeO_2$. The main reaction in the leaching process is shown as:

$$3LiMeO_2 + Al + 12H^+ \rightarrow 3Li^+ + Al^{3+} + 3Me^{2+} + 6H_2O \quad (12)$$

The side reaction in the leaching process is shown as:

$$2Al + 6H^+ \rightarrow 2Al^{3+} + 3H_2 \quad (13)$$

The electron reduction efficiency α is calculated by the following equation, and since the amount of electrons transferred per reaction of 3 mol $LiMeO_2$ is the same as that of the reaction of 1 mol Al, the correspondence is regulated by the coefficient 3:

$$\alpha = \frac{n_{Me}}{3n_{Al}} 100\% \quad (14)$$

where n_{Al} and n_{Me} represent the amounts of Al and the sum of the amounts of Ni, Co and Mn in the leaching solution, respectively, and their units are mol. The sum of the amounts of Ni, Co and Mn represents the amount of electrons involved in the main reaction, while three times the amount of Al represents the total amount of electrons released from Al foils. As α gets closer to 1, it shows that more Al foils are directly involved in the reduction of the high-valent transition metal oxides, while a smaller α represents that more Al is involved in the side reaction. It should be noted that the quality of the Al foil and positive electrode powder in the raw materials used in this study are shown in Fig. S24. Calculations indicate that the molar ratio of Al is ~18% excessive. As the thickness and quality of Al foil in commercial LIBs continue to decrease[42], this ratio will gradually decrease, which also means that this galvanic leaching strategy will remain effective for a long time to come.

Material characterization

A field emission scanning electron microscope (FE-SEM, Hitachi SU-8010, Japan) was employed to capture the surface morphology of NCM electrodes and organic framework during the galvanic leaching process. Inductively coupled plasma optical emission spectroscopy (ICP-OES, PerkinElmer, OPTIMA 2000, USA) was employed to analyze the concentration of dissolved metals to calculate the elemental composition. XRD (Philips PW 1700, USA) was employed to explore the lattice evolution during the galvanic leaching process. In order to capture the coupling characteristics of the Al foils and the NCM particles, we took out the NCM electrode strips during the galvanic leaching process, cured them into the resin, and sanded and polished them to expose the smooth cross-section as shown in Fig. S25. FE-EPMA (8050G, Shimadzu, Japan) was employed to analyze the element content on these smooth cross-sections, to obtain the elemental distribution of remaining NCM particles and Al foils. XPS (Thermo Fisher, Escalab 250Xi, USA) with an argon ion etching gun was used to explore for changes in elemental valence states in the surface layer of particles from the surface to the bulk, under a monochromated Al Kα source and at an energy of 1486.6 eV. XANES analysis was supported by Hefei Light Source, and the obtained XAFS data was processed in Athena for background, pre-edge line and post-edge line calibrations.

Data availability

All the data generated in this study are provided in the Supplementary Information/ Source Data file. Source data are provided with this paper.

References

1. Heenan, T. M. M. et al. Mapping internal temperatures during high-rate battery applications. *Nature* **617**, 507–512 (2023).
2. Lee, M. J. et al. Elastomeric electrolytes for high-energy solid-state lithium batteries. *Nature* **601**, 217–222 (2022).
3. Wang, J. X. et al. Sustainable upcycling of spent $LiCoO_2$ to an ultra-stable battery cathode at high voltage. *Nat. Sustain.* **6**, 797–805 (2023).
4. Baars, J., Domenech, T., Bleischwitz, R., Melin, H. E. & Heidrich, O. Circular economy strategies for electric vehicle batteries reduce reliance on raw materials. *Nat. Sustain.* **4**, 71–79 (2021).
5. Qiu, B. et al. Waste plastics upcycled for high-efficiency H_2O_2 production and lithium recovery via Ni-Co/carbon nanotubes composites. *Nat. Commun.* **15**, 6473 (2024).
6. Olivetti, E. A., Ceder, G., Gaustad, G. G. & Fu, X. K. Lithium-ion battery supply chain considerations: analysis of potential bottlenecks in critical metals. *Joule* **1**, 229–243 (2017).
7. Vierunketo, M., Klemettinen, A., Reuter, M. A., Santasalo-Aarnio, A. & Serna-Guerrero, R. A multi-dimensional indicator for material and energy circularity: Proof-of-concept of exentropy in Li-ion battery recycling. *Iscience* **26**, 108237 (2023).
8. Harper, G. et al. Recycling lithium-ion batteries from electric vehicles. *Nature* **575**, 75–86 (2019).
9. Yu, J. et al. A promising physical method for recovery of $LiCoO_2$ and graphite from spent lithium-ion batteries: Grinding flotation. *Sep. Purif. Technol.* **190**, 45–52 (2017).
10. Zhang, Y. et al. Application of Falcon centrifuge in the recycling of electrode materials from spent lithium ion batteries. *J. Clean. Prod.* **202**, 736–747 (2018).
11. Zhong, X. H. et al. Pyrolysis and physical separation for the recovery of spent $LiFePO_4$ batteries. *Waste Manage* **89**, 83–93 (2019).
12. Shan, M. H. et al. Recycling of $LiFePO_4$ cathode materials: from laboratory scale to industrial production. *Mater. Today* **73**, 130–150 (2024).
13. Yu, J. et al. Mechanochemical upcycling of spent $LiCoO_2$ to new $LiNi_{0.80}Co_{0.15}Al_{0.05}O_2$ battery: an atom economy strategy. *Proc.Natl Acad. Sci. USA* **120**, e2217698120 (2023).

14. Yu, J. et al. In-situ enhanced catalytic reforming behavior of cobalt-based materials with inherent zero-valent aluminum in spent lithium ion batteries. *Appl. Catal. B Environ.* **303**, 120920 (2022).
15. Yu, J. D., Tan, Q. Y. & Li, J. H. Exploring a green route for recycling spent lithium-ion batteries: Revealing and solving deep screening problem. *J. Clean. Prod.* **255**, 120269 (2020).
16. Chernyaev, A. et al. The efficiency of scrap Cu and Al current collector materials as reductants in LIB waste leaching. *Hydrometallurgy* **203**, 105608 (2021).
17. Peng, C., Liu, F. P., Aji, A. T., Wilson, B. P. & Lundström, M. Extraction of Li and Co from industrially produced Li-ion battery waste - Using the reductive power of waste itself. *Waste Manage* **95**, 604–611 (2019).
18. Joulie, M., Billy, E., Laucournet, R. & Meyer, D. Current collectors as reducing agent to dissolve active materials of positive electrodes from Li-ion battery wastes. *Hydrometallurgy* **169**, 426–432 (2017).
19. Wang, M. et al. Recycling spent lithium-ion batteries using a mechanochemical approach. *Circular Economy* **1**, 100012 (2022).
20. Liu, K., Tan, Q., Yu, J. & Wang, M. A global perspective on e-waste recycling. *Circular Economy* **2**, 100028 (2023).
21. Liu, Y. Y. et al. Rechargeable aqueous Zn-based energy storage devices. *Joule* **5**, 2845–2903 (2021).
22. Zhu, J. G. et al. A method to prolong lithium-ion battery life during the full life cycle. *Cell Rep. Phys. Sci.* **4**, 101464 (2023).
23. Wang, H. L. et al. Efficient direct repairing of lithium- and manganese-rich cathodes by concentrated solar radiation. *Nat. Commun.* **15**, 1634 (2024).
24. Chen, B. C. et al. Room-temperature salt template synthesis of nitrogen-doped 3D porous carbon for fast metal-ion storage. *Angew. Chem. Int. Ed.* **63**, e202316116 (2024).
25. Tang, D. et al. A multifunctional amino acid enables direct recycling of spent $LiFePO_4$ cathode material. *Adv. Mater.* **36**, 2309722 (2024).
26. Shi, R. Y. et al. Homogeneous repair of highly degraded Ni-rich cathode material with spent lithium anode. *Adv. Mater.* **36**, 2311553 (2024).
27. Jia, K. et al. Topotactic transformation of surface structure enabling direct regeneration of spent lithium-ion battery cathodes. *J. Am. Chem. Soc.* **145**, 7288–7300 (2023).
28. Edge, J. S. et al. Lithium ion battery degradation: what you need to know. *Phys. Chem. Chem. Phys.* **23**, 8200–8221 (2021).
29. Xu, J. G., Deshpande, R. D., Pan, J., Cheng, Y. T. & Battaglia, V. S. Electrode side reactions, capacity loss and mechanical degradation in lithium-ion batteries. *J. Electrochem. Soc.* **162**, A2026–A2035 (2015).
30. Xu, R., Sun, H., de Vasconcelos, L. S. & Zhao, K. J. Mechanical and structural degradation of $LiNi_xMn_yCo_zO_2$ cathode in Li-ion batteries: an experimental study. *J. Electrochem. Soc.* **164**, A3333–A3341 (2017).
31. Ungár, T., Gubicza, J., Ribárik, G., Pantea, C. & Zerda, T. W. Microstructure of carbon blacks determined by X-ray diffraction profile analysis. *Carbon* **40**, 929–937 (2002).
32. Mi, L. W. et al. A nest-like $Ni@Ni_{1.4}Co_{1.6}S_2$ electrode for flexible high-performance rolling supercapacitor device design. *J. Mater. Chem. A* **3**, 20973–20982 (2015).
33. Chen, Y. M. et al. Database of ab initio L-edge X-ray absorption near edge structure. *Sci. Data* **8**, 153 (2021).
34. Wang, J. L. et al. In situ X-ray spectroscopies beyond conventional X-ray absorption spectroscopy on deciphering dynamic configuration of electrocatalysts. *Nat. Commun.* **14**, 6576 (2023).
35. Ma, J. et al. Subtractive transformation of cathode materials in spent Li-ion batteries to a low-cobalt 5 V-class cathode material. *Nat. Commun.* **15**, 1046 (2024).
36. Xu, P. P. et al. Efficient direct recycling of lithium-ion battery anoodes by targeted healing. *Joule* **4**, 2609–2626 (2020).
37. Culcasi, A., Gueccia, R., Randazzo, S., Cipollina, A. & Micale, G. Design of a novel membrane-integrated waste acid recovery process from pickling solution. *J. Clean. Prod.* **236**, 117623 (2019).
38. Merkel, A. et al. Recovery of hydrochloric acid from industrial wastewater by diffusion dialysis using a spiral-wound module. *Int. J. Mol. Sci.* **23**, 6212 (2022).
39. Yu, J. D. et al. Unveiling sodium ion pollution in spray-dried precursors and its implications for the green upcycling of spent lithium-ion batteries. *Environ. Sci. Technol.* **55**, 14897–14905 (2021).
40. Wang, M. M. et al. Integrated assessment of deep eutectic solvents questions solvometallurgy as a sustainable recycling approach for lithium-ion batteries. *One Earth* **6**, 1400–1413 (2023).
41. Liu, K. et al. Low-carbon recycling of spent lithium iron phosphate batteries a hydro-oxygen repair route. *Green Chem* **25**, 6642–6651 (2023).
42. Zhu, P. et al. A review of current collectors for lithium-ion batteries. *J. Power Sources* **485**, 229321 (2021).

Acknowledgements

We are grateful to Dr. Wang Mengmeng and Dr. Liu Kang from the Department of Civil and Environmental Engineering at Hong Kong Polytechnic University for their help in the XANES analysis, to Dr. Zhang Beikai, Dr. Song Duanmei and Dr. Wu Jing from the School of Environment in Tsinghua University for their help in the experimental research and data analysis. We are very grateful to Dr. Shi Yang from GEM (Wuxi) Energy Material Co., Ltd. for collaborating with us in the development and cycling performance testing of Al-doped ternary positive electrode materials. We would like to thank Shuo Li from Xueyanhui Scientific Research Platfrom (www.xueyanhui.com) for the XPS analysis, to eceshi (www.eceshi.com) for the HRTEM test. We confirm that this research is supported by the National Natural Science Foundation of China (52300162, Y.J.D. and 52270127, L.J.H.). The financial support for this project comes from legal channels.

Author contributions

J.Y. performed various advanced characterization analyses, carried out techno-economic studies, and wrote the manuscript. Y.L. carried out leaching experiments and provided a kinetic theoretical analysis. J.L. conceived and supervised the project. All the authors contributed to the whole manuscript.

Competing interests

The authors declare no competing interests.

Additional information

Supplementary information The online version contains supplementary material available at https://doi.org/10.1038/s41467-025-57857-9.

Correspondence and requests for materials should be addressed to Jinhui Li.

Peer review information *Nature Communications* thanks Toyohisa Fujita, and the other, anonymous, reviewer(s) for their contribution to the peer review of this work. A peer review file is available.